

# Multi-Cycle Large Eddy Simulation (LES) of the Cycle-to-Cycle Variation (CCV) of Spark Ignition (SI) - Controlled Auto-Ignition (CAI) Hybrid Combustion in a Gasoline Engine

Author, co-author (Do NOT enter this information. It will be pulled from participant tab in MyTechZone)

Affiliation (Do NOT enter this information. It will be pulled from participant tab in MyTechZone)

Copyright © 2017 SAE International

## Abstract

The spark ignition (SI) – controlled auto-ignition (CAI) hybrid combustion, also known as spark-assisted compression ignition (SACI), is achieved by utilizing the temperature and pressure rise from the early flame propagation induced by the spark-ignition to trigger the auto-ignition of the remaining unburned mixture. This hybrid combustion concept can be used to effectively extend the operating range of gasoline CAI combustion and achieve smooth transitions between SI and CAI combustion mode in gasoline engines. However, the significant cycle-to-cycle variation (CCV) of the SI-CAI hybrid combustion hinders the practical application of the hybrid combustion. In order to understand the cause of its high CCVs, the SI-CAI hybrid combustion process in a gasoline engine was studied in this study by the large eddy simulations (LES). The turbulence is modelled by the sub-grid k model. The spark ignition and subsequent flame propagation were modelled by the ECFM-3Z LES model. A tabulated database of the gasoline auto-ignition chemistry was coupled with the CFD simulations to depict the subsequent auto-ignition process of the unburned mixture after the initiation of flame propagation. The LES simulation was validated and applied to analyze the hybrid combustion process in a single cylinder engine at 1500 rpm and 5.43 bar IMEP, which was characterized with a coefficient of variation (COV) of 11.81% in IMEP. The LES simulations of 15 consecutive cycles were performed and analyzed to evaluate the potential of LES simulations to predict the CCV of SI-CAI hybrid combustion. The analysis of the LES simulation results indicates that the average thermal and compositional parameters are not the main reason for the cycle-to-cycle variations of the SI-CAI hybrid combustion. The temperature and residual gas fraction (RGF) in the spark zone is also very stable among different cycles. In comparison, the average velocity in the whole cylinder reduces from 7.8 m/s in the strong combustion cycle (Cycle 11) to 6.4 m/s in the weakest combustion cycle (Cycle 14) with 21.9% reduction, and the average velocity in the spark zone reduces from 6.3 m/s to 3.8 m/s with 60.3% reduction. Therefore, the variations of the in-cylinder flow velocity, especially around the spark plug, could be the main reason for the large variations of the hybrid combustion observed in the experiments.

## Introduction

Although the controlled auto-ignition (CAI) combustion produces higher fuel conversion efficiency and ultra-low NO<sub>x</sub> emission, the

high sensitivity of combustion process to the boundary conditions and its narrow operation range have prevented it from being adopted in production engines [1]. The spark ignition (SI) has been introduced into the CAI combustion concept to assist the control of auto-ignition over extended engine operating conditions [2, 3]. The SI-CAI hybrid combustion, also known as spark assisted compression ignition (SACI), can produce higher thermal efficiency and lower NO<sub>x</sub> emissions than the traditional SI combustion whilst it produces lower heat release rate and wider load operation range than the pure CAI combustion [4]. Furthermore, this hybrid combustion concept would also facilitate the smooth transitions between pure SI mode and CAI mode [4-8].

The SI-CAI hybrid combustion is achieved by utilising the temperature and pressure rise due to the early flame propagation induced by the spark ignition to trigger the auto-ignition of the remaining unburned mixture. The hybrid combustion process comprises two different combustion modes and involves complex interactions between the early flame propagation and subsequent auto-ignition process. This in turn leads to significant cycle-to-cycle variations of hybrid combustion at some engine operating conditions [4, 9-15]. Chen et. al [4] observed the high cycle-to-cycle variations of the hybrid combustion during the mode transition from homogeneous charge compression ignition (HCCI) combustion mode to SI mode and the authors attributed the main reason to the thermal oscillations among cycles. At some load conditions, significant cycle-to-cycle variations were observed in the peak cylinder pressure, the maximum rate of heat release and the timings of peak cylinder pressure and peak heat release, although the SI-CAI hybrid combustion exhibited relatively low cyclic variations in the engine's output as measured by the COV of IMEP [9]. Wagner et. al [10, 11] observed the high cyclic combustion variability during the transition between propagating flame combustion and homogeneous charge compression ignition (HCCI) in a single-cylinder spark-assisted gasoline engine and suggested that the nonlinear EGR feedback is probably the major source of the observed variations after the comparisons with previous studies of lean-limit cyclic variations. Sen et. al [12] found that the heat release variations were very small in amplitude and exhibited more persistent low-frequency oscillations in both the spark-ignition combustion mode and HCCI combustion mode, while a wide range of very large-amplitude oscillations occurred, including both persistent low-frequency periodicities and intermittent high-frequency bursts at intermediate states between SI and HCCI. Larimore et. al [13] analyzed and modeled the engine behavior of high cycle-to-cycle variations of spark assisted auto-ignition (SACI)

combustion and found that a control oriented model which captures the recycled thermal and chemical energy may be sufficient to describe the process. In order to capture the instability during the SI-HCCI transition, Havstad et.al. [15] applied a CHEMKIN-based multi-zone model with a 63-species reaction mechanism and mass and energy balances for the cylinder and the exhaust flow. They found the fluctuations of exhaust gas recirculation (EGR) level, average cylinder temperature, zone-to-zone temperature and intake pressure are mainly responsible to the combustion oscillations with hybrid combustion mode.

The application of the computational fluid dynamics (CFD) simulations to describe the SI-CAI hybrid combustion process also provides some insights to understand the origin of the CCV of hybrid combustion. Joellson et.al. [16] analyzed the effect of the initial in-cylinder temperature and turbulence conditions on the spark assisted compression ignition (SACI) by means of large eddy simulations (LES) and found the turbulence plays a significant role in the first stage SI flame propagation whereas the initial temperature governs the second stage HCCI process. The two-dimensional direct numerical simulations (DNS) performed by Yoo et.al. [17] showed that the high flow turbulence significantly enhances the overall combustion of SACI combustion by inducing many deflagration waves. Wang et. al [18-23] investigated the effects of in-cylinder thermal stratification, flow motions and fuel stratifications on the SI-CAI hybrid combustion process and found that the hybrid combustion is especially sensitive to the local turbulence kinetic energy (TKE) [21], velocity magnitude [20, 21], temperature [18, 19, 21], temperature inhomogeneity [21] and fuel/air equivalence ratio [22, 23] around the spark plug.

Although the above studies have identified some causes that could lead to the cycle-to-cycle variations of hybrid combustion process by the observations of the experimental results and chemical kinetic modeling study, there is no consensus on the dominant factors leading to the high CCV of SI-CAI hybrid combustion. The single-cycle CFD simulations only confirm some key factors that would affect the hybrid combustion, and the origins of the high CCV of hybrid combustion in a real engine application is still unclear. In this study, the multi-cycle large eddy simulations (LES) of the SI-CAI hybrid combustion are performed and compared with the experiments to explore the origins of CCV of hybrid combustion. The simulation results are analyzed in detail to understand the variations of in-cylinder conditions, fame propagation and auto-ignition process and their contributions to the variation of the whole combustion process.

## Single Cylinder Engine Experiment

The experiments were carried out on a single cylinder gasoline engine and the engine specifications are shown in Table 1. The engine comprises a Ricardo Hydra single cylinder block and a specially designed cylinder head, which is equipped with a 4-variable valve actuation system (4VVAS) with BMW's Vanos and Valvetronics on both the intake and exhaust camshafts [2, 4]. The 4VVAS enables the continuous adjustment of intake/exhaust valve lift and the valve timing. Both external exhaust gas recirculation (EGR) and internal EGR were used to achieve the SI-CAI hybrid combustion. The internal EGR was achieved by utilizing the negative valve overlapping (NVO) strategy. In this study, an engine operating point with coefficient of variation (COV) of 11.81% in IMEP at 1500 rpm and 5.43 bar IMEP (in average of 100 cycles) was selected. The valve parameters for the 4VVAS, including intake/exhaust valve opening timing (IVO/EVO), closing timing (IVC/EVC) and lift (IL/EL), are presented in Table 2. The average value of the total residual gas fraction (RGF) after the intake valve closing (IVC) is around 25% in the experiments.

Table 1. Engine specifications.

Bore	86 mm
Stroke	86 mm
Displacement	0.5 L
Geometric compression ratio	10.66
Combustion chamber	Pent roof / 4 valves
Fuel injection	Port fuel injection
Fuel	Gasoline 93 RON
Intake pressure	Naturally aspirated
Throttle	WOT

Table 2. Engine operating conditions.

EVO/ EVC [°CA]	167 / 383
EL [mm]	2.3
IVO / IVC [°CA]	411 / 593
IL [mm]	2.7
Spark Timing [°CA]	671
Fuel/air equivalence ratio [-]	1
Coolant temperature[°C]	85
Oil temperature [°C]	55
Engine speed [r/min]	1500
Fueling Rate [mg/cycle]	22.4
IMEP [bar]	5.43

## Engine Simulation setup

### Numerical models

The multi-cycle large eddy simulations (LES) were performed in STAR-CD software. The sub-grid k model [24, 25] was used to model the flows and turbulence. The standard wall treatment was implemented to model the near-wall turbulence in LES simulations. The SI-CAI hybrid combustion comprises both early flame propagation and subsequent auto-ignition process. A set of models for the premixed flame propagation and auto-ignition combustion were employed to cover both the turbulent mixing effects and chemical kinetics in the hybrid combustion. Basing on our previous Reynolds-averaged Navier–Stokes (RANS) simulations of SI-CAI hybrid combustion [20], the three-zones extended coherent flame model (ECFM3Z) for LES [26], which can consider premixed flame propagation, diffusion flame propagation and auto-ignition combustion, was adopted as the framework of the hybrid combustion model. The gas state in ECFM3Z is represented by a pure fuel zone, a pure air plus possible residual gas zone and a mixed zone [27]. The mixed zone, where the combustion takes place, is the result of the turbulent and molecular mixing between gases in the other two zones. The flame surface density equation was used to describe the flame

propagation process and predict the reaction rate of the flame propagation. The average flame surface density is defined as the local area of flame per unit of volume ( $m^{-1}$ ), which is used to describe the intensity of flame propagation. The tabulated chemistry approach [28] was adopted to predict the auto-ignition of the unburned charge. Chemical kinetic calculations under various thermodynamic and dilution conditions (temperature: 480-1520 K, pressure: 1-60 bar, equivalence ratio: 0.2-3 and residual gas fraction: 0-90%) were performed with a reduced gasoline surrogate mechanism [29] to construct the tabulated database of the auto-ignition delay time. In this case, the tabulated database is coupled with the CFD simulations by look-up tables so that the central processing unit (CPU) time requirement is significantly reduced compared with the CFD simulations directly coupled with the chemical kinetic mechanism. With the tabulated chemistry approach, the auto-ignition tendency was defined to explicitly describe the close degree of fresh mixture from auto-ignition in each cell, and the value of 0 indicates no tendency to auto-ignition and the value of 1 indicates the occurrence of auto-ignition. Then, the reaction rate of the auto-ignition combustion can be determined by the combustion characteristic time.

During the calculation, the reaction regime of each cell is determined by the average flame surface density and the auto-ignition tendency. The available fuel/air mixture in a cell will be consumed by the flame propagation according to the flame surface density equation when the local average flame surface density of the cell is greater than 0. By contrast, the available fuel/air mixture in a cell will be consumed by auto-ignition combustion according to the tabulated chemistry approach if the auto-ignition tendency of the cell achieves 1. The species concentrations in the combustion are determined by the reaction rates of the flame propagation and auto-ignition, respectively. The application of above models enables the prediction of the SI-CAI hybrid combustion. The detailed modelling of SI-CAI hybrid combustion basing on the above concept can be found in a previous paper [20].

### Simulation conditions

The adopted initial and boundary conditions in CFD simulations are shown in Table 3. In the simulations, the inconsistency of the wall temperature of the cylinder head, the piston surface and the cylinder liner was considered. The temperature of the cylinder liner and the piston is evaluated by the cylinder head temperature and coolant temperature [19]. The intake mixture from the inlet boundary was set as the homogeneous fuel/air mixture with the stoichiometric equivalence ratio due to the adoption of the port fuel injection and the burned exhaust gas at the same external EGR rate with experiments. The intake mixture would come into the cylinder and mix with the in-cylinder residual gas (completely burned gas) once the intake valve opens. The CFD simulations were carried out from 400 °CA before top dead center (bTDC) just before the intake valve opening (IVO) timing and throughout the following 15 burning cycles.

Table 3. Simulation conditions.

<i>Initial conditions @ 400 °CA ATDC for 1<sup>st</sup> cycle</i>	
Cylinder temperature [K]	664
Cylinder pressure [bar]	0.4
Intake temperature [K]	320
Intake pressure [bar]	0.985
Exhaust temperature [K]	865

Exhaust pressure [bar]	1.02
<b>Boundary conditions</b>	
Intake temperature [K]	320
Intake pressure [bar]	0.95
Exhaust temperature [K]	913
Exhaust pressure [bar]	1.03
Cylinder head temperature [K]	420
Spark plug temperature [K]	800
Piston top temperature [K]	482
Cylinder liner temperature [K]	377

### Numerical method and engine mesh

The Pressure-Implicit with Splitting of Operators (PISO) algorithm was used to solve the equations. The equations of momentum, turbulence kinetic energy and turbulence dissipation were discretized with the monotone advection and reconstruction scheme (MARS). The upwind differencing scheme (UD) and central differencing scheme (CD) were applied to discretize the temperature and density equations, respectively. The residual tolerance for the momentum, turbulence kinetic energy and turbulence dissipation was set at 0.001 while the residual tolerance for pressure and temperature was set at 0.0001 to achieve good compromise between convergence and computational time. The angular time-step in the simulations was fixed at 0.05 degree crank angle.

The engine mesh was generated in ES-ICE software and several cylinder cell layers of the moving mesh were automatically deleted/added during the compression/expansion stroke. The arbitrary sliding interface (ASI) was applied to control the connectivity between the intake and exhaust domains and the cylinder domain with the movement of the valves. The moving mesh of the engine for the LES simulations are shown in Figure 1. There are around 870,000 grids with 0.96 mm averaged grid size at bottom dead center (BDC) and 550,000 grids with 0.79 mm average grid size at top dead center (TDC), respectively. The mesh around the spark plug is refined with 0.6 mm grid size in order to predict the spark ignition and early flame propagation process.

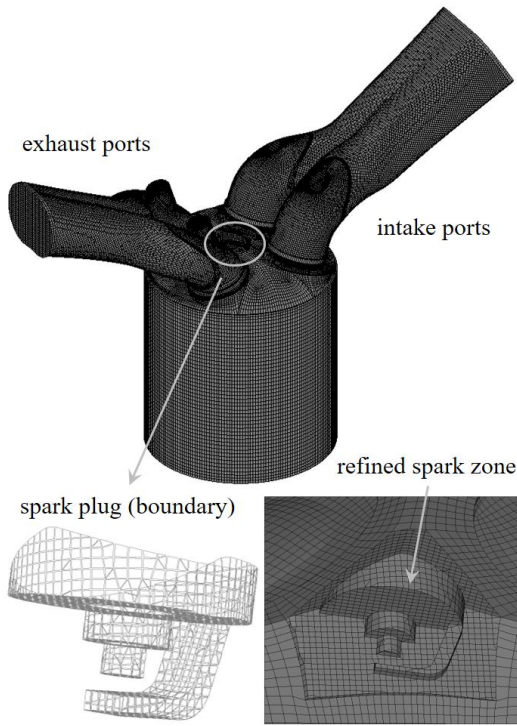


Figure 1. Engine mesh.

In order to assess the applicability of the LES results, the distributions of the turbulence resolution parameter ( $M$ ) proposed by Pope [30] were shown in Figure 2 at different crank angles.  $M$  is the ratio of the sub-grid scale (SGS) kinetic energy to the total kinetic energy. The turbulence resolution with  $M$  of 0 denotes a direct numerical simulation (DNS) simulation where all turbulence scales are resolved, and the  $M$  of 1 denotes a RANS simulation where no turbulence scales are resolved and all are modelled. It was recommended that a turbulence resolution parameter  $M$  should be less than 0.2 for an adaptive LES simulation [30]. It is noted that the turbulence resolution parameter  $M$  is significantly lower than 0.2 during the LES simulations in this study. The region around the spark plug gap shows the highest turbulence resolution with  $M$  around 0.1 due to the poorer mesh of the spark region with the complex geometric features.

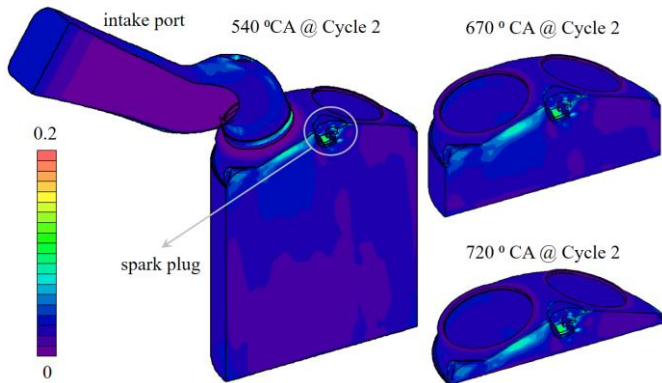


Figure 2. Distributions of turbulence resolution parameter  $M$  during the LES simulations.

## Results and discussion

### Comparison between experiments and the LES simulations

Figure 3 compares the pressure traces of the engine experiments and the corresponding LES simulation results. The grey band, as shown in the figure, compassed by the lower and upper limit of the pressure trace in the experiments indicates strong cycle-to-cycle variations of the combustion process of the SI-CAI hybrid combustion. The pressure traces of the LES simulations are shown by the solid curves with different colors in the figure. Overall, the LES simulations could reproduce the cycle-to-cycle variations of the pressure trace very well. However, it is noted that the hybrid combustion process close to the experimental lower limit (almost misfire) is not predicted very well by the current LES modeling.

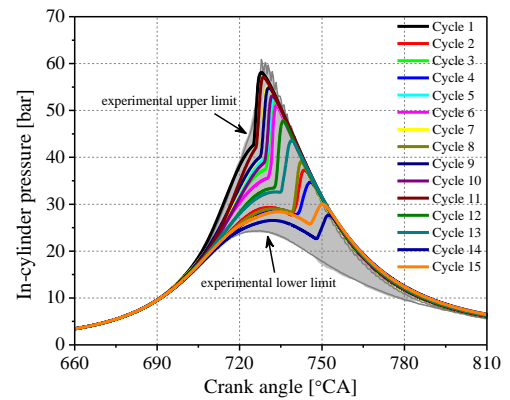


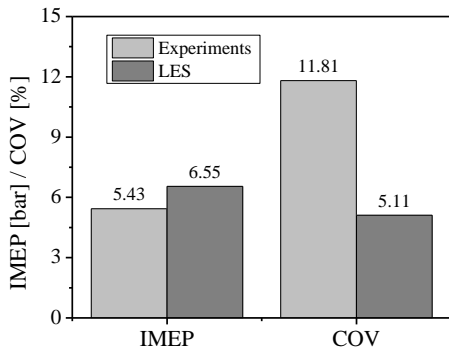
Figure 3 compares the pressure traces between the experiments and 15 cycles LES simulations.

In order to quantitatively define the degree of the cycle-to-cycle variation of the combustion process, the coefficient of variation (COV) of IMEP and peak pressure (PP) are calculated and shown in Figure 4. The equation of the COV is shown as following:

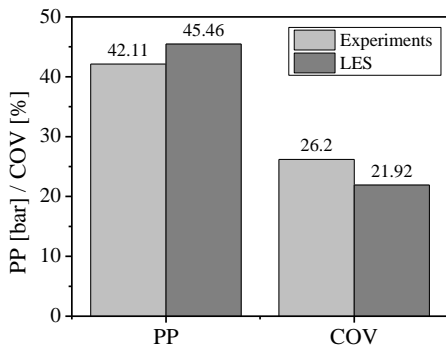
$$\text{COV} = \frac{\text{standard deviation}}{\text{mean value}} \times 100\% \quad (1)$$

It should be noted that the first cycle (Cycle 1) of the LES simulations is excluded for the data analysis in order to minimize the impact of the initial simulation conditions on the results. As shown in Figure 4 (a), the predicted average IMEP with LES simulations is 6.55 bar, which is higher than the average IMEP of experiments at 5.43 bar. This in turn leads to smaller cycle-to-cycle variations of the IMEP by LES simulations. As shown in the Figure 4 (a), the predicted COV of IMEP is 5.11%, which is only half of the experimental COV of IMEP at 11.81%.

In Figure 4 (b), the comparison of the average peak pressure (PP) and the corresponding COV shows a fairly good agreement between the experiments and LES simulations. The predicted average peak pressure is 45.46 bar, which is slightly higher than the experimental observation at 42.11 bar. The predicted COV of PP is 21.92 %, which is slightly lower than the experimental COV at 26.2%.



(a)



(b)

Figure 4. Comparison of the average values and COVs of (a) IMEP, (b) peak pressure (PP) from experiments and LES.

Figure 5 compares the scatter plot of the IMEP of the current cycle and next cycle in experiments and LES simulations. Although the pressure traces of the LES simulations fall into the experimental envelop, as shown in Figure 3, most of predicted IMEP points locate at upper right side of the experimental results, indicating faster and more sufficient combustion processes of the LES simulations. However, the experiments and LES simulations show similar cycle-to-cycle variation patterns which have the most points located along the upper and right boundary.

Figure 6 shows the IMEP histograms of the consecutive cycles obtained by experiments and LES simulations. The y-axis “cycle number” refers to the total number of the cycles within a specific range of IMEP on the x-axis. It is noted that there are more cycles with higher IMEP values concentrating at right part of the distribution in both experiments and LES simulations. A smaller number of cycles of lower IMPE values disperses over a wider region in the left part of the distribution.

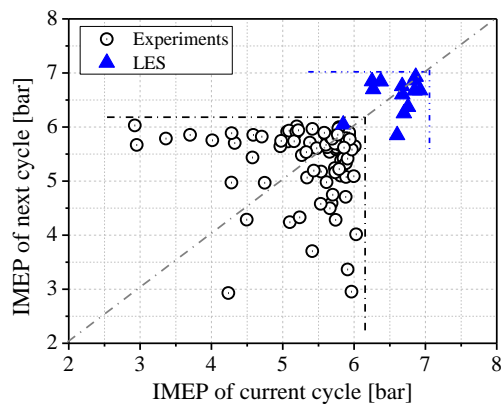


Figure 5. Comparison of the scatter plot of the IMEP of the current cycle and next cycle in experiments and LES simulations.

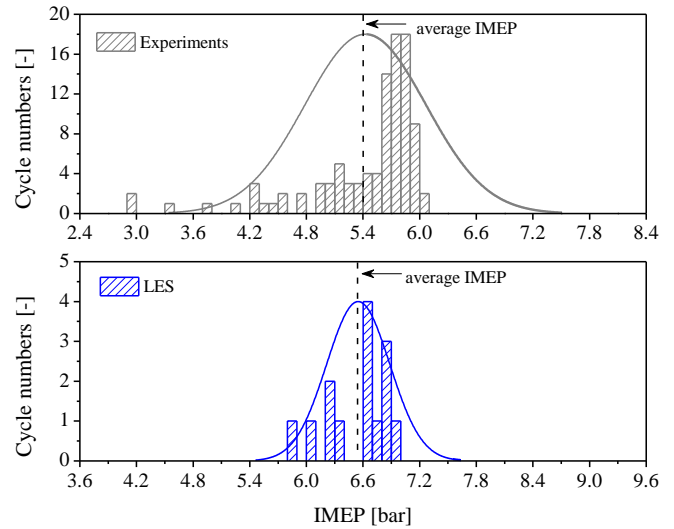


Figure 6. Comparison of the IMEP histograms of the consecutive cycles obtained by experiments and LES simulations.

Figure 7 and 8 compare the scatter plots of the peak pressure (PP) and the histograms of PP in experiments and LES simulations. Although the sample scale of the LES simulations is small, the predicted scatter plot of PP, as show in Figure 7, shows a very discrete distribution pattern, which is similar to the experimental results. In Figure 8, it is noted that there are two peaks of the distributions of PP at both lower PP values (~30 bar) and high PP values (~55 bar) in the experiments, while only one peak is observed for the LES simulations at PP around 55 bar in Figure 8.

According to the above analysis and comparison, the discrepancy between the experimental results and LES simulations of the SI-CAI hybrid combustion can be attributed to the following reasons:

1. The weak hybrid combustion cycle, which is close to the lower limit of experimental observations in Figure 3, is not well predicted by LES simulations. In addition to the small sample scale of current study (only 14 LES cycles), the simplified spark ignition model used in this study could be the reason and a more advanced model, e.g. Arc and Kernel Tracking ignition model (AKTIM) [31] and Imposed Stretch Spark ignition model (ISSIM) [32], might be useful to improve the prediction.
2. The combustion rate and the sufficiency of combustion process are over-predicted, which lead to higher IMEP values of the LES simulations. The possible reason of this could be the accuracy of the prediction of the transition from SI to CAI combustion [20] and the thermal stratifications caused by the wall temperature which affect the later CAI combustion rate [18, 19].

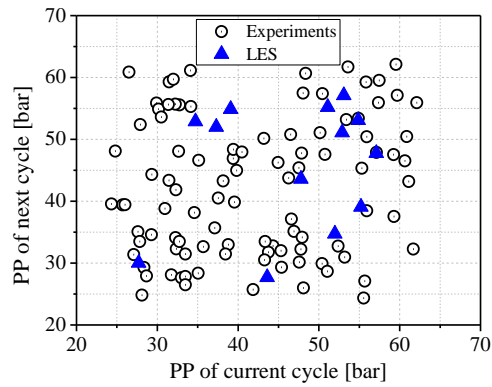


Figure 7. Comparison of the scatter plot of the peak pressure (PP) of the current cycle and next cycle in experiments and LES simulations.

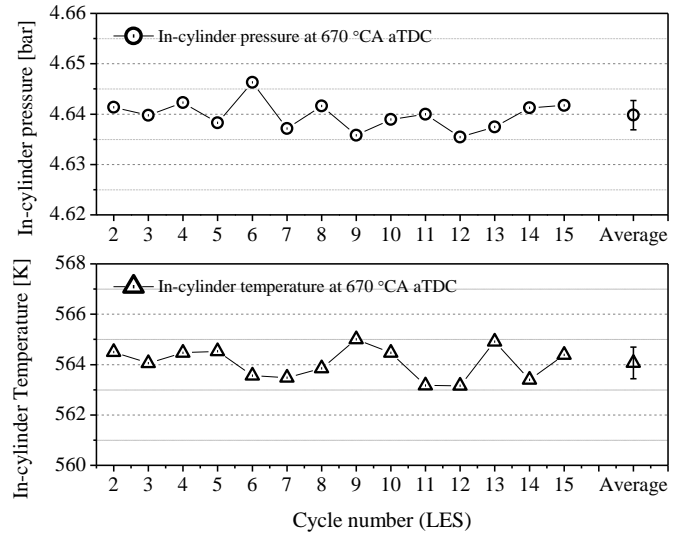


Figure 9. In-cylinder average pressure and temperature for each cycle, and their average values and standard deviations at 670 °CA aTDC.

The in-cylinder charge mass and the composition before the spark ignition are also the potential causes of the cycle-to-cycle variations of the combustion process. However, it is found that both in-cylinder total mass and the composition are very stable among cycles, as shown in Figure 10. The total in-cylinder mass is around 481 mg with standard deviation of 0.56 mg, while the average external EGR (eEGR) and internal EGR (iEGR) are stabilized at 0.06 and 0.2, respectively.

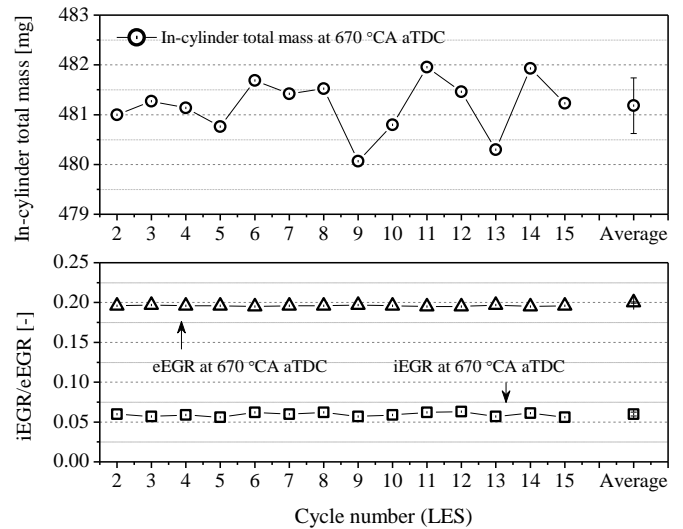


Figure 10. In-cylinder total mass of the charge, iEGR and eEGR for each cycle, and their average values and standard deviations at 670 °CA aTDC.

The analysis of those average parameters shown in Figure 9 and 10 indicates that the average thermal and compositional parameters are not the main reason for the large cycle-to-cycle variations of SI-CAI hybrid combustion. Therefore, the main reasons could be zone to zone thermal and compositional distributions and flow field in the cylinder. Three typical cycles, i.e. Cycle 11 with the strongest combustion process, Cycle 13 with a moderate combustion process and Cycle 14 with the weakest combustion process, are selected for the detail analysis. The mass fraction burned (MFB) profiles of these three cycles are shown in Figure 11. It is obvious that the difference of the

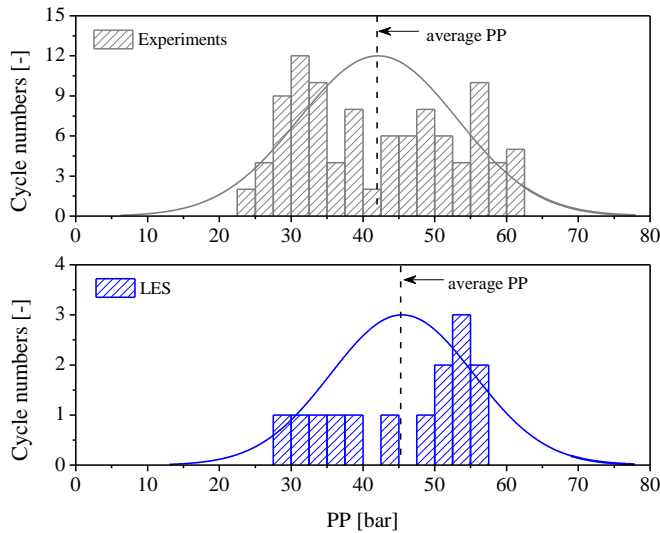


Figure 8. Comparison of the histograms of the peak pressure (PP) of the current cycle and next cycle in experiments and LES simulations.

### Analysis of the CCVs of hybrid combustion

In this section, the cycle-to-cycle variations predicted by the LES simulations are analyzed in detail. Figure 9 compares the average pressure and temperature for each cycle at 670 °CA aTDC just before the spark ignition timing. The average values and standard deviations are also shown in the figure. The average in-cylinder pressure is 4.64 bar and the standard deviation is as low as 0.003 bar, as shown in Figure 9. The experimental results actually show similar trend that the average in-cylinder pressure at 670 °CA is 4.77 bar with the standard deviation of 0.069 bar. The average in-cylinder temperature before the spark ignition is also very stable among different cycles. The predicted average temperature is around 564 K with standard deviation of 0.63 K. Therefore, it is found that the average in-cylinder pressure and temperature before the spark ignition are very stable regardless the strong variations of the subsequent combustion processes observed in Figure 3.

hybrid combustion begins at the very beginning, i.e. at the SI stage, and gradually expands with the combustion process. The combustion phasing (CA 50, crank angle of 50% MFB) gradually delays from 6.25 °CA aTDC in Case 11 to 27.95 °CA aTDC in Case 14. The IMEP correspondingly decreases from 7.09 bar in Case 11 to 5.99 bar in Case 14.

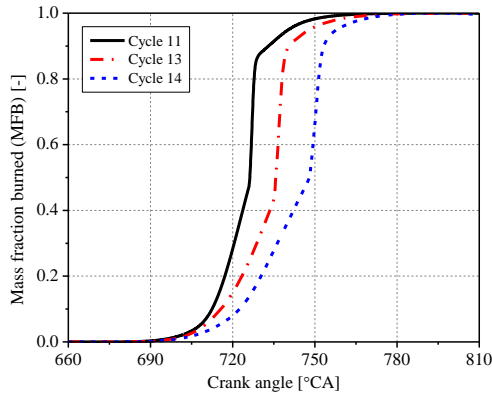


Figure 11. The evolutions of the mass burned fraction (MFB) for the selected three cycles: Cycle 11, Cycle 13 and Cycle 14.

Figure 12 and 13 compare section views of the in-cylinder temperature and total residual gas fraction (RGF) distributions respectively. The mixture around the spark plug shows higher temperature due to the hotter spark plug. Although there are some differences of the temperature distributions, especially at the spark plug region and near-wall region among three cases, the difference of the temperature in the intermediate region is very slight. The RGF distribution patterns in different cycles are very different, as shown in Figure 13, while the RGF are overall homogeneous (the scale in the figure is 0.25 to 0.26). A spherical zone with 3 mm diameter around the spark plug gap is defined as spark zone to understand the variations of conditions around the spark plug. As shown in Figure 14, it is noted that both the temperature and RGF show very slight changes in different cycles. The temperature in the spark zone is increased from 570 K in Cycle 11 to 573 K in Cycle 14 and RGF decreases from 0.257 in Cycle 11 to 0.255 in Cycle 13.

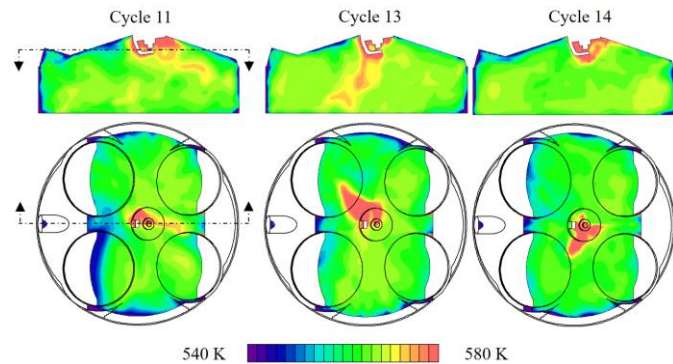


Figure 12. In-cylinder temperature distributions for Cycle 11, Cycle 13 and Cycle 14 at 670 °CA aTDC.

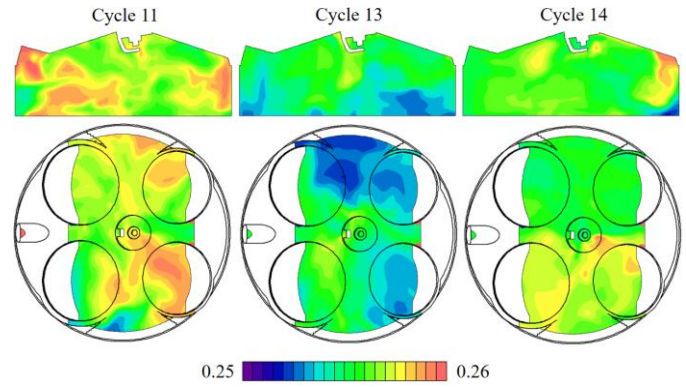


Figure 13. In-cylinder RGF distributions for Cycle 11, Cycle 13 and Cycle 14 at 670 °CA aTDC.

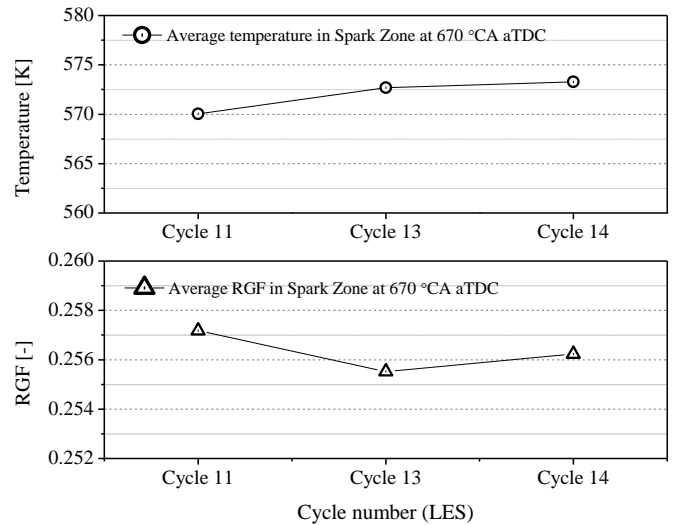
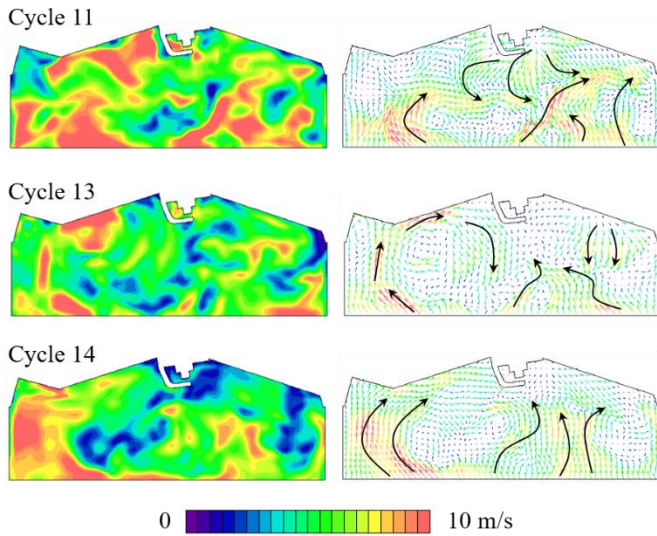
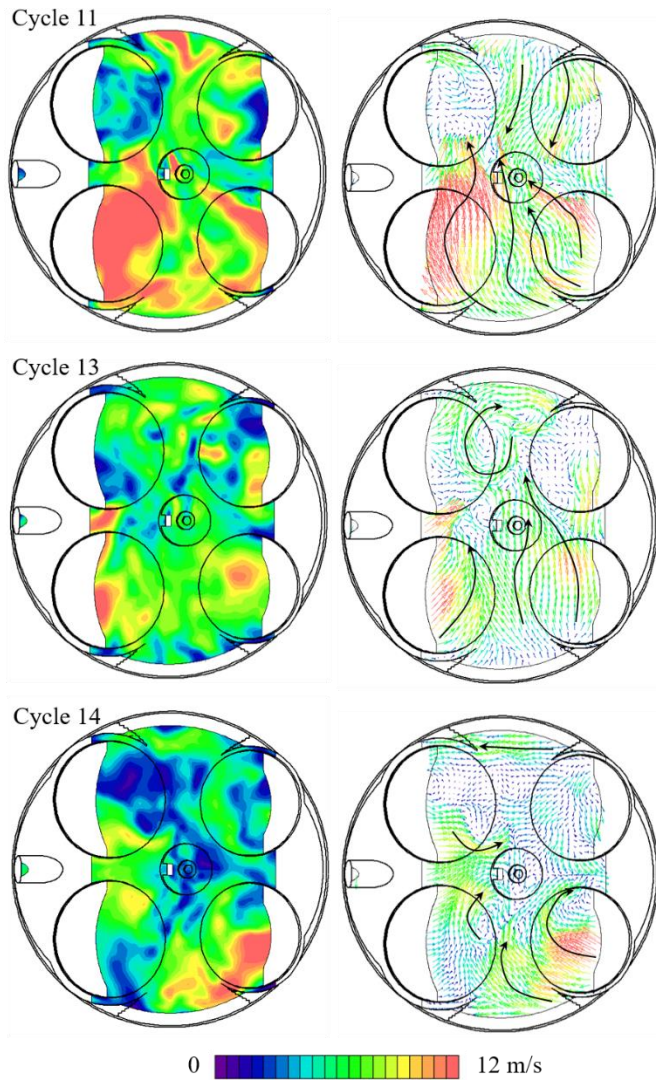


Figure 14. The average temperature and total RGF in the spark zone for Cycle 11, Cycle 13 and Cycle 14 at 670 °CA aTDC.

Figure 15 compares the in-cylinder velocity magnitude (left) and vector (right) at 670 °CA aTDC. Overall, the high velocity area for the strong combustion cycle (Cycle 11) is larger, as shown by the velocity magnitude distributions. In addition, strong flow motions across the spark plug gap are also observed in Cycle 13. However, the velocity around the spark plug is very weak for the weakest combustion cycle (Cycle 14), and the high velocity region is mainly distributed at the outer region. Figure 16 quantitatively shows the average velocity in the whole cylinder and spark zone at 670 °CA aTDC. The average velocity in the whole cylinder reduces from 7.8 m/s in Cycle 11 to 6.4 m/s in Cycle 14 with 21.9% reduction, and the average velocity in the spark zone reduces from 6.3 m/s to 3.8 m/s with 60.3% reduction. Therefore, the variations of the in-cylinder flow velocity, especially around the spark plug, could be the main reason for the large variations of the hybrid combustion observed in the experiments.



(a)



(b)

Figure 15. Distributions of the velocity magnitude (left) and vector (right) at 670 °CA aTDC in the (a) vertical section and (b) horizontal section for Cycle 11, Cycle 13 and Cycle 14 at 670 °CA aTDC.

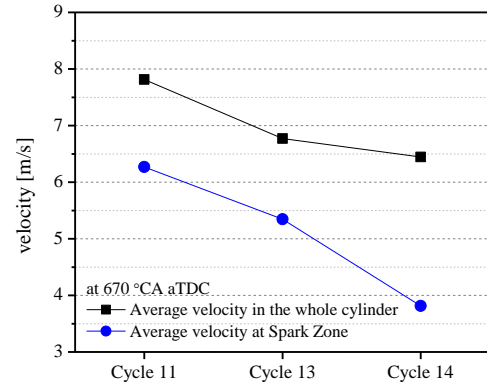


Figure 16. The average velocity magnitude in the whole cylinder and spark zone for Cycle 11, Cycle 13 and Cycle 14 at 670 °CA aTDC.

Figure 17 shows the section views of the in-cylinder flame surface density distributions at 720 °CA for different cycles. In the strongest combustion cycle (Cycle 11), the irregular flame front has expanded to the whole combustion chamber at TDC under the strong enhancement of the in-cylinder flow fields. In comparison, the flame propagation is much weaker in Cycle 14 and mainly concentrates around the spark plug.

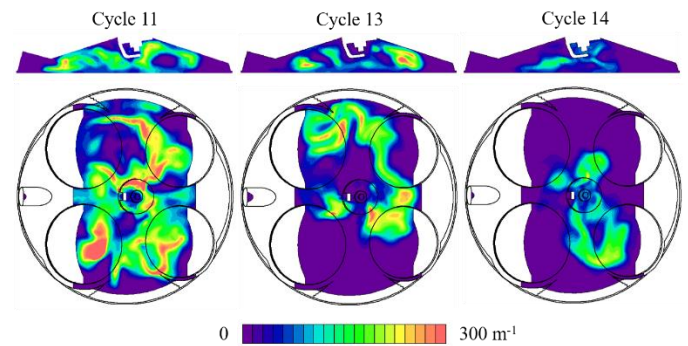


Figure 17. Comparison of the flame surface density distribution for Cycle 11, Cycle 13 and Cycle 14 at 720 °CA aTDC.

Figure 18 shows the distributions of the auto-ignition tendency for Cycle 11 and 13. The crank angle of the distribution is different for each cycle to ensure similar mass burned fraction with 87.7% MFB at 730 °CA in Cycle 11 and 89.2% MFB at 740 °CA in Cycle 13. As defined in the Section Numerical models, the auto-ignition tendency is used to describe the degree of the mixture close to the auto-ignition. The auto-ignition tendency of 1 indicates the occurrence of auto-ignition and a larger value (>1) indicates the earlier auto-ignition process. Compared to the slower combustion cycle (Cycle 13), the faster flame propagation in Cycle 11 leads to more auto-ignition sites and these auto-ignition regions mainly locate at the outer region of the cylinder with more unburned charge, which contributes to overall faster combustion rate of Cycle 11.

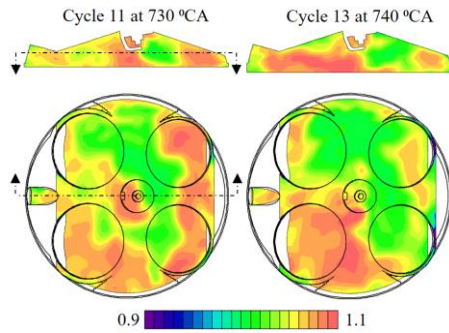


Figure 18. Comparison of the auto-ignition tendency distribution for Cycle 11 and Cycle 13.

## Conclusions

In this study, the multi-cycle large eddy simulations (LES) of the SI-CAI hybrid combustion process were performed and analyzed to understand the large cycle-to-cycle variations of the hybrid combustion. The sub-grid  $k$  model [24, 25] was used to model the flows and turbulence. The three-zones extended coherent flame model (ECFM3Z) for LES [26] was adopted as the framework of the hybrid combustion model. The flame surface density equation was used to describe the flame propagation process. The tabulated chemistry approach [28] was adopted to predict the auto-ignition of the unburned charge.

It is found that the predicted average IMEP with LES simulations is 6.55 bar, which is higher than the average IMEP of experiments at 5.43 bar, while the predicted COV of IMEP is 5.11%, which is only half of the experimental COV of IMEP at 11.81%. The prediction of the peak pressure by LES simulations shows promising agreements that the predicted average peak pressure is 45.46 bar, which is slightly higher than the experimental observation at 42.11 bar. The predicted COV of PP is 21.92 %, which is slightly lower than the experimental COV at 26.2%.

The discrepancy between the experimental results and LES simulations of the SI-CAI hybrid combustion can be attributed to the following reasons:

1. The weak hybrid combustion cycle, which is close to the lower limit of experimental observations, is not well predicted by LES simulations. In addition to the small sample scale of current study (only 14 LES cycles), the simplified spark ignition model used in this study could be the reason and a more advanced model, e.g. Arc and Kernel Tracking ignition model (AKTIM) [31] and Imposed Stretch Spark ignition model (ISSIM) [32], might be useful to improve the prediction.
3. The combustion rate and the sufficiency of combustion process are over-predicted, which leads to higher IMEP values of the LES simulations. The possible reason of this could be the accuracy of the prediction of the transition from SI to CAI combustion [20] and the thermal stratifications caused by the wall temperature which affect the later CAI combustion rate [18, 19].

The analysis of the LES simulation results indicates that the average thermal and compositional parameters are not the main reason for the cycle-to-cycle variations of SI-CAI hybrid combustion. The temperature and residual gas fraction (RGF) in the spark zone is also very stable among different cycles. In comparison, the variations of the in-cylinder flow velocity, especially around the spark plug, are very

significant among different cycles, which could be the main reason for the large variations of the hybrid combustion observed in the experiments.

The LES simulation results show that in the strongest combustion cycle (Cycle 11), the irregular flame front has expanded to the whole combustion chamber at TDC under the strong enhancement of the in-cylinder flow fields. The faster flame propagation then leads to more auto-ignition sites and these auto-ignition regions mainly locate at the outer region of the cylinder with more unburned charge, which contributes to overall faster combustion rate.

The preliminary attempt of applying the multi-cycle LES simulations of SI-CAI hybrid combustion in this study shows the potential to understand the large cycle-to-cycle variations of SI-CAI hybrid combustion by means of LES simulations. More work will be done in near future to resolve the discrepancy between modeling and experiments found in this study.

## References

1. Zhao, H., HCCI and CAI engines for the automotive industry. 2007, Cambridge, England: Woodhead Publishing.
2. Xie, H., et al., The Effect of Spark Ignition on the CAI Combustion Operation. 2005, SAE Technical Paper 2005-01-3738.
3. Wang, Z., et al., Effects of Spark Ignition and Stratified Charge on Gasoline HCCI Combustion With Direct Injection. 2005, SAE Technical Paper 2005-01-0137.
4. Chen, T., et al., Continuous Load Adjustment Strategy of a Gasoline HCCI-SI Engine Fully Controlled by Exhaust Gas. 2011, SAE Technical Paper 2011-01-1408.
5. Milovanovic, N., et al., SI-HCCI-SI Mode Transition at Different Engine Operating Conditions. 2005, SAE Technical Paper 2005-01-0156.
6. Santoso, H., J. Matthews and W.K. Cheng, Managing SI/HCCI Dual-Mode Engine Operation. 2005, SAE Technical Paper 2005-01-0162.
7. Zhang, Y., H. Xie and H. Zhao, Investigation of SI-HCCI Hybrid Combustion and Control Strategies for Combustion Mode Switching in a Four-Stroke Gasoline Engine. *Combust. Sci. and Tech.*, 2009. 181: p. 782–799.
8. Manofsky, L., et al., Bridging the Gap between HCCI and SI: Spark-Assisted Compression Ignition, in SAE Technical Paper 2011-01-1179. 2011.
9. Chen, T., et al., Analysis of cyclic variations during mode switching between spark ignition and controlled auto-ignition combustion operations. *International Journal of Engine Research*, 2015. 16(3): p. 356–365.
10. Wagner, R.M., et al., On the Nature of Cyclic Dispersion in Spark Assisted HCCI Combustion, in SAE. 2006, SAE Technical Paper 2006-01-0418.

11. Daw, C.S., et al., Understanding the transition between conventional spark-ignited combustion and HCCI in a gasoline engine. *Proceedings of the Combustion Institute* 31, 2007. 31: p. 2887–2894.
12. Sen, A.K., et al., Characteristics of cyclic heat release variability in the transition from spark ignition to HCCI in a gasoline engine. *Applied Energy*, 2012. 88: p. 1649–1655.
13. Larimore, J., et al., Experiments and Analysis of High Cyclic Variability at the Operational Limits of Spark-Assisted HCCI Combustion. 2012, American Control Conference (ACC) 2012; 12\_ACCb. p. 2072 - 2077.
14. Temel, V.K. and J. Sterniak, Characterization of SACI Combustion for Use in Model Based Controls. 2014, SAE Technical Paper 2014-01-1289.
15. Havstad, M.A., et al., Detailed Chemical Kinetic Modeling of Iso-octane SI-HCCI Transition. 2010, SAE Technical Paper 2010-01-1087.
16. Joelsson, T., R. Yu and X.S. Bai, Large Eddy Simulation of Turbulent Combustion in a Spark-Assisted Homogenous Charge Compression Ignition Engine. *Combustion Science and Technology*, 2012. 184: p. 1051–1065.
17. Yoo, C.S., et al., A DNS study of ignition characteristics of a lean iso-octane/air mixture under HCCI and SACI conditions. *Proceedings of the Combustion Institute*, 2013. 34(2): p. 2985-2993.
18. Wang, X., et al., Effect of the Thermal Stratification on SI-CAI Hybrid Combustion in a Gasoline Engine. *Applied Thermal Engineering*, 2013. 61(2): p. 451–460.
19. Wang, X., et al., Wall Temperature Effect on SI-CAI Hybrid Combustion Progress in a Gasoline Engine. 2013, SAE Technical Paper 2013-01-1662.
20. Wang, X., et al., Numerical simulation and validation of SI-CAI hybrid combustion in a CAI/HCCI gasoline engine. *Combustion Theory and Modelling*, 2013. 17(1): p. 142-166.
21. Wang, X., H. Xie and H. Zhao, Computational study of the influence of in-cylinder flow on spark ignition–controlled auto-ignition hybrid combustion in a gasoline engine. *International Journal of Engine Research*, 2015. 16(5): p. 795-809.
22. Wang, X., H. Zhao and H. Xie, Effect of piston shapes and fuel injection strategies on stoichiometric stratified flame ignition (SFI) hybrid combustion in a PFI/DI gasoline engine by numerical simulations. *Energy Conversion and Management*, 2015. 98(0): p. 387 - 400.
23. Wang, X., H. Zhao and H. Xie, Effect of dilution strategies and direct injection ratios on Stratified Flame Ignition (SFI) hybrid combustion in a PFI/DI gasoline engine. *Applied Energy*, 2016. 165: p. 801–814.
24. Speziale, C.G., Analytical methods for the development of Reynolds-stress closures in turbulence. *Annual Review of Fluid Mechanics*, 1991. 23(1): p. 107-157.
25. Cd-adapco, Methodology, STAR-CD VERSION 4.14, 2010. 2010.
26. Vermorel, O., et al., Towards the understanding of cyclic variability in a spark ignited engine using multi-cycle LES. *Combustion and Flame*, 2009. 156(8): p. 1525-1541.
27. Colin, O. and A. Benkenida, The 3-Zones Extended Coherent Flame Model (ECFM3Z) for Computing Premixed/Diffusion Combustion. *Oil & Gas Science and Technology*, 2004. 59(6): p. 593-609.
28. CRUZ, A.P.D., Three-dimensional modeling of self-ignition in HCCI and conventional diesel engines. *Combustion Science and Technology*, 2004. 176(5-6): p. 867-887.
29. Mehl, M., et al., An approach for formulating surrogates for gasoline with application towards a reduced surrogate mechanism for CFD engine modeling. *Energy & Fuels*, 2011. 25(11): p. 5215-5223.
30. Pope, S.B., Ten questions concerning the large-eddy simulation of turbulent flows. *New journal of Physics*, 2004. 6(1): p. 35.
31. Vermorel, O., et al., Towards the understanding of cyclic variability in a spark ignited engine using multi-cycle LES. *Combustion and Flame*, 2009. 156: p. 1525–1541.
32. Colin, O. and K. Truffin, A spark ignition model for large eddy simulation based on an FSD transport equation (ISSIM-LES). *Proceedings of the Combustion Institute*, 2011. 33: p. 3097-3104.

## Contact Information

Dr. Xinyan Wang  
 xinyan.wang@brunel.ac.uk  
 Centre for Advanced Powertrain and Fuel Research  
 Brunel University London, UK  
 UB8 3PH

## Acknowledgments

The authors would like to acknowledge Dr Tao Chen and Prof. Hui Xie in State Key Laboratory of Engines (SKLE), Tianjin University for their inputs of the experimental work in this paper.